Advances in Geo-Energy Research

Vol. 19, No. 3, p. 201-215, 2026

Original article

Intelligent facies modeling of shallow-water delta reservoirs with conditional generative adversarial networks

Changsheng Lu[1]*, Junbang Liu[2], Shaohua Li[1], Gang Hui[3]*, Shengnan Chen[4], Mengjiao Dou[1]

[1]*School of Geosciences, Yangtze University, Wuhan 430100, P. R. China*

[2]*PetroChina Research Institute of Petroleum Exploration, Beijing 100083, P. R. China*

[3]*State Key Laboratory of Petroleum Resources and Engineering, China University of Petroleum, Beijing 102249, P. R. China*

[4]*Department of Chemical and Petroleum Engineering, University of Calgary, Calgary, AB T2N1N4, Canada*

Keywords:
Generative adversarial networks
sedimentary facies modeling
shallow-water delta
artificial intelligence
deep learning

Cited as:
Lu, C., Liu, J., Li, S., Hui, G., Chen, S., Dou, M. Intelligent facies modeling of shallow-water delta reservoirs with conditional generative adversarial networks. Advances in Geo-Energy Research, 2026, 19(3): 201-215. https://doi.org/10.46690/ager.2026.03.01

Abstract:
Accurate geological modeling of shallow-water delta reservoirs remains challenging due to complex sedimentary architecture and strong heterogeneity. This study develops an advanced modeling technique that integrates geological process understanding with deep learning, with a focus on the accurate representation of channel geometry under multiple data constraints. Field outcrop investigations of the Chang 6 Member in the Ordos Basin were conducted to clarify key geological characteristics and geometric parameters of shallow-water distributary channels. An improved object-based method was employed to effectively generate three-dimensional training datasets capturing typical channel bifurcation and convergence patterns. A conditional progressive generative adversarial network is proposed to incorporate multi-source constraints, including global geological features, well logs, and seismic probability volumes, thereby enabling simultaneous learning of geological patterns and data fidelity. Application to a shallow-water delta reservoir in the Ordos Basin demonstrates that the method produces geologically realistic facies models that honor all available constraints, significantly improving modeling accuracy and computational efficiency. This work provides an innovative and adaptive methodology for intelligent modeling of complex reservoir systems.

1. Introduction

Geological modeling is fundamental in oil and gas exploration and development, seeking to recreate the three-dimensional (3D) structure and property distribution of subsurface reservoirs by amalgamating geological insights with diverse data sources, such as well logs, drilling, and seismic information (Yang et al., 2024a; Liu et al., 2025). This reconstruction offers essential assistance for reservoir characterization (Cai et al., 2020; Du and Bai, 2024; Ren et al., 2025), numerical modeling (Zhao et al., 2024; Bao et al., 2025; Tang et al., 2026), and development planning (Li et al., 2017; Zheng et al., 2022). Traditional geostatistical methodologies, including sequential indicator simulation (Hui et al., 2021; Hui et al., 2025; Zhao et al., 2025), object-based approaches (Deutsch and Wang, 1996; Deutsch and Tran, 2002), process-based techniques (Pyrcz et al., 2009; Jia et al., 2024), and multi-point geostatistical methods (Mariethoz and Caers, 2014; Tahmasebi, 2018; Wang et al., 2021), frequently demonstrate deficiencies in accurately replicating authentic geological patterns.

In recent years, generative adversarial networks (GANs) have achieved extensive utilization in domains including image synthesis and 3D modeling, owing to their ability to comprehend spatial structures and produce extremely realistic sampl-

*Corresponding author.
E-mail address: luchangsheng@yangtzeu.edu.cn (C. Lu); liujunbang@petrochina.com.cn (J. Liu); lish@yangtzeu.edu.cn (S. Li); hui.gang@cup.edu.cn (G. Hui); snchen@ucalgary.ca (S. Chen); doumj0302@163.com (M. Dou).

Received December 8, 2025; revised January 10, 2026; accepted February 2, 2026; available online February 5, 2026.

Yandy Scientific Press

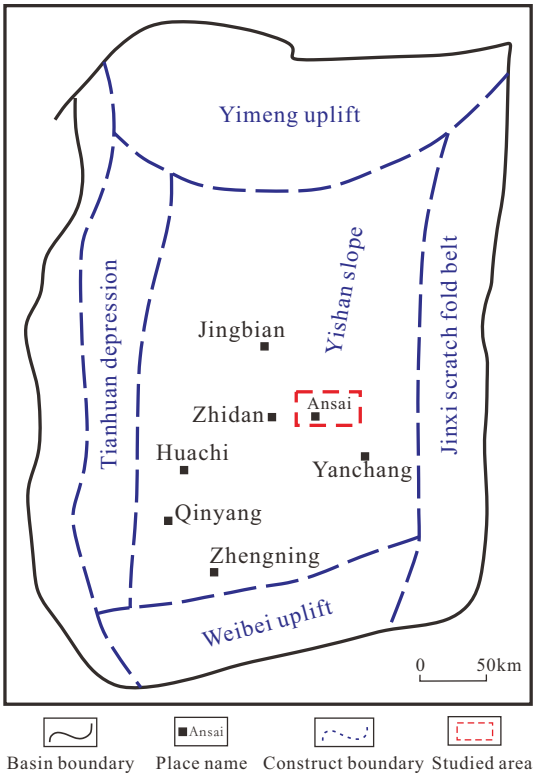

Fig. 1. Location map of AS Oilfield in the Ordos Basin.

es (Mao et al., 2020; Liu et al., 2021b; Dong et al., 2022; Murgas et al., 2024; Chen et al., 2025). Since the initial introduction of reservoir modeling by Laloy et al. (2017), researchers have consistently enhanced GAN architectures and training methodologies (Kavousinejad et al., 2025), systematically investigating their applicability for geological modeling (Song et al., 2021a, 2021b; Chen et al., 2022). Compared to traditional multi-point geostatistical methods, GANs can autonomously extract multi-scale geological features from training images, demonstrating enhanced adaptability and generalization capabilities in non-stationary contexts and intricate sedimentary environments (Zhang et al., 2022). They demonstrate enhanced pattern reproduction capabilities and increased computing efficiency. Progressive GANs have been effectively utilized across various reservoir types, including fluvial channels (Zhang et al., 2019), braided rivers (Zhang et al., 2025), paleo-karst caves (Wang et al., 2025), and fault-controlled karst systems (Hui et al., 2023, 2024; Hu et al., 2024).

Nonetheless, two significant hurdles remain in the use of GANs to reservoir modeling. The quality of training samples fundamentally dictates the network's generative performance; however, the assembly of high-quality training image datasets for intricate sedimentary facies, such as shallow-water deltas, remains inadequately developed (Lu et al., 2024). Secondly, reservoir models must accurately replicate geological configurations and adhere to multi-source restrictions derived from well and seismic data. Successfully incorporating these limitations into the network architecture and training process continues to be a significant problem in GAN-based modeling (Song et al., 2021b).

This study examines the shallow-water delta reservoirs in the WY Block of the AS Oilfield to tackle these problems. This study utilizes a conditional progressive generative adversarial network (CPGAN) to accomplish integrated modeling that encompasses global geological characteristics, well data, and seismic limitations. This study presents an innovative methodology and a technical framework for utilizing GANs in the simulation of shallow-water delta reservoirs.

2. Field background

The WY Block of the AS Oilfield is located within the Zhidan-WY nose-shaped uplift in the Ordos Basin. The region features a very uncomplicated structural framework, mostly governed by a west-dipping monocline. At the conclusion of the Triassic Period, the Indosinian Movement caused significant uplift and erosion in the basin, resulting in the development of the Jurassic sedimentary system (Fig. 1) (Zhu et al., 2017; Hou et al., 2021). The Yanchang Formation exemplifies a typical lacustrine-deltaic sedimentary sequence, illustrating the cyclical enlargement and reduction of the lake alongside fluctuations in sediment deposition across its stratigraphic range from bottom to top (Liu et al., 2021a; Yang et al., 2024b).

The Chang 6 Member is a significant reservoir interval within the Yanchang Formation. During its deposition, the lake basin diminished while deltaic systems proliferated due to increased sediment supply, leading to a depositional environment characterized by shallow-water delta facies. The distribution of sand bodies in the Chang 6 oil-bearing interval is predominantly influenced by subaqueous distributary channels, exhibiting a gradual tendency of aggradation and forward migration from the Chang 6^3 to the Chang 6^1 submembers. The studied area is characterized by delta front subfacies, where reservoirs typically demonstrate low porosity, low permeability, and significant heterogeneity (Huang et al., 2014; Chen et al., 2015; Qi et al., 2024).

During the Chang 6 interval of the WY Block, delta front subfacies are present, characterized by significant sedimentary microfacies such as subaqueous distributary channels, mouth bars, distributary bays, and sheet sands. Subaqueous distributary channels constitute the primary sandstone framework in the region, exhibiting grain sizes from medium-fine sand to silt and frequently demonstrating repeated fining-upward cycles; associated well-log responses typically reveal serrated box- or bell-shaped patterns. Mouth bars are distinguished by consistent grain size and a reasonably pure sandstone composition, typically displaying coarsening-upward sequences in vertical profiles, accompanied by funnel-shaped log traces. Distributary bays primarily comprise fine-grained mudstones with low-amplitude log responses. Sheet sands are laterally extensive but thin, generally occurring along channel margins or adjacent to sand bars (Fig. 2).

Planar sedimentary microfacies maps reveal that the reservoir sand bodies in the studied area are primarily constituted of subaqueous distributary channels and their corresponding mouth bars. Marginal deposits develop along channel flanks, while distal areas contain minor mouth bar and sheet sand ac-

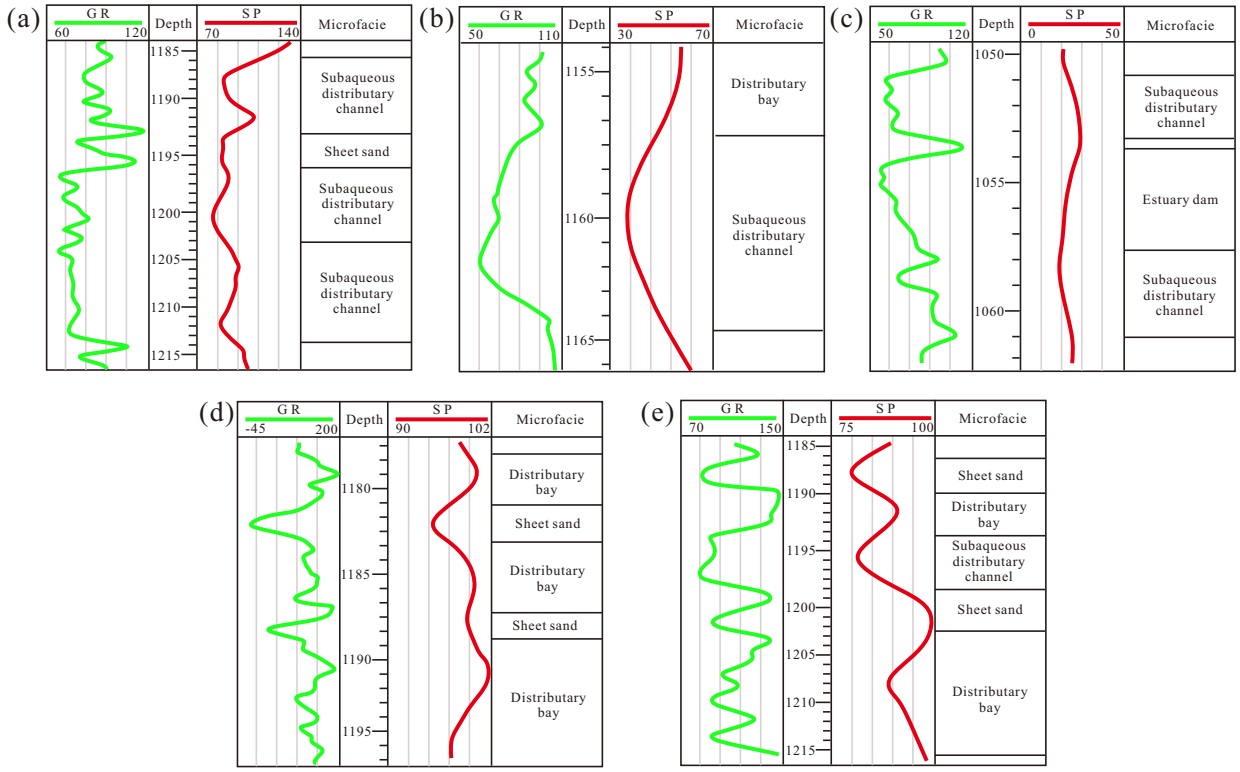

Fig. 2. Well log response characteristics of shallow water delta sedimentary microfacies. (a) W8-15 distributary bay, (b) W13-28 subaqueous distributary channel, (c) W16-156 estuary dam and (d) W8-15 distributary bay and (e) W266-16 sheet sand.

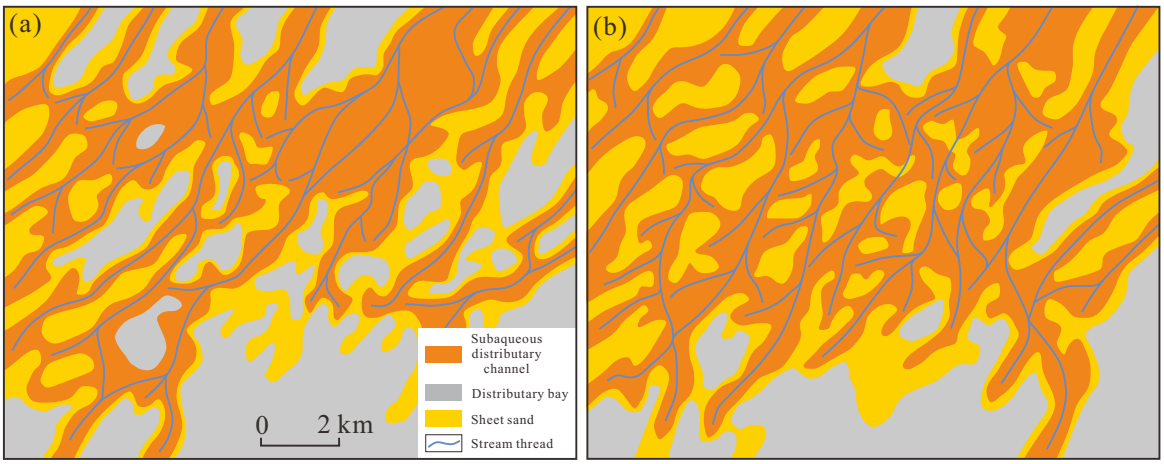

Fig. 3. Planar distribution map of sedimentary microfacies in the Yanchang Formation: (a) Sedimentary microfacies plan of the Chang6^{1-2-4} and (b) sedimentary microfacies plan of the Chang6^{1-2-3}.

cumulations. The spatial distribution and evolutionary patterns of these sedimentary units are influenced by the intensity of sediment delivery and variations in lake levels (Fig. 3).

3. Methodology

3.1 Constructing conceptual models of subaqueous distributary channels

3.1.1 Design of the training dataset algorithm

Training datasets are crucial for the effective use of artificial intelligence approaches, including GANs, as they furnish the fundamental foundation for models to comprehend geological patterns and produce realistic reservoir models. In light of the lack of a specialized facies-model dataset for shallow-water delta reservoirs in the AS Oilfield, a focused approach was devised to create conceptual models of subaqueous distributary channels, including their lateral boundaries. This approach relies on previously documented depositional patterns (Fig. 4(a)). The channel system was constructed based on the schematic depicted in Figs. 4(b) and 4(c), whereby sheet sands and mouth bars are included into laterally adjacent channel edges. This design yields three microfacies types:

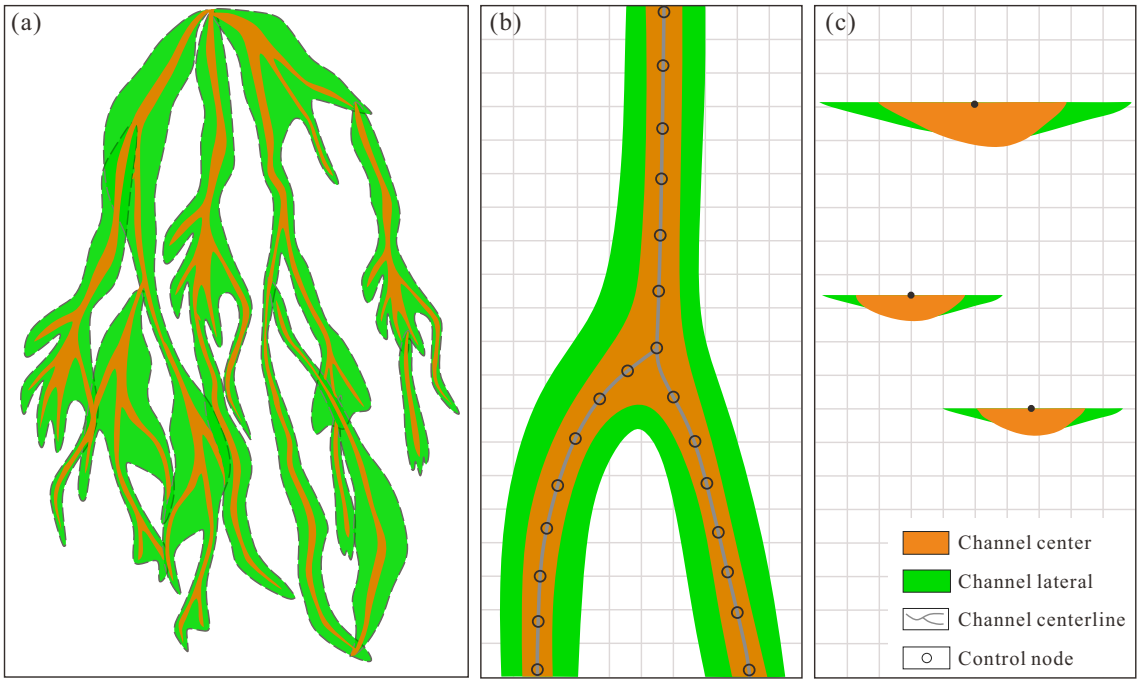

Fig. 4. Design pattern of subaqueous distributary channels. (a) The map of the subaqueous distributary channel geological model, (b) the plane of a subaqueous distributary channel and (c) the cross section of a subaqueous distributary channel.

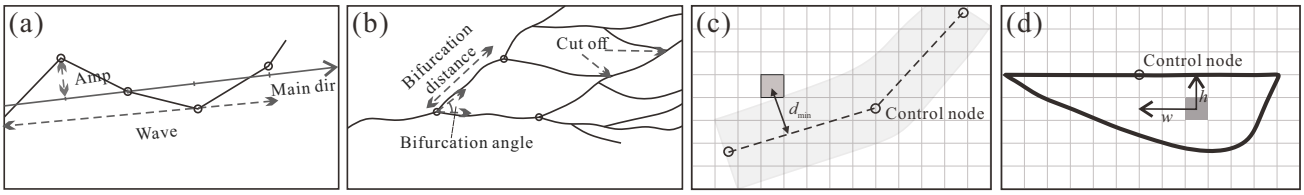

Fig. 5. Vector object-based representation of shallow water delta channels. (a) Vectorization of the centerline of the channel, (b) fork and truncation of the centerline, (c) the planar relationship between river objects and grids and (d) the vertical relationship between river objects and grids.

(1) Subaqueous distributary main channel, (2) lateral channel margin, and (3) distributary bay. The primary channel body and its lateral edges possess a common regulating centerline. The cross-section reveals that the lateral borders possess a broad, slender geometry, in contrast to the thicker, narrower morphology of the main channel body (Fig. 4).

3.1.2 Vector-based channel object definition and simulation

This research improves the simulation methodology for subaqueous distributary channels by advancing the object-based fluvial modeling technique of Fluvsim and incorporating a tailored design framework for shallow-water delta systems. The enhanced technique incorporates 3D vector line entities to depict distinct channels within a singular depositional phase. Spatial vector relationships are utilized to objectively assess bifurcation and convergence attributes between channels. This method accurately replicates sedimentary processes characterized by numerous interconnected channels with frequent bifurcation and convergence occurrences (Fig. 5). In contrast to the conventional Fluvsim technique, the employment of vector line objects facilitates an accurate delineation of channel centerlines and their interconnections. This breakthrough addresses prior constraints in managing complex channel crossings and truncations, facilitating more precise simulation of the convoluted evolution characteristic of shallow-water delta distributary systems.

The channel centerline is depicted as a vector line consisting of control points (Fig. 5(a)), defined by amplitude (lateral deviation from the main channel axis) and wavelength (length of one complete oscillation cycle). Channel bifurcation is quantitatively characterized by three factors (Fig. 5(b)): Mean bifurcation distance (threshold for triggering bifurcation events), bifurcation angle (angular divergence between progeny channels), and bifurcation direction (directional deviation from the parent channel). Upon bifurcation, the parent channel is immobilized and included into the centerline collection, with its terminal node acting as the origin for daughter channels. Simulation concludes when channels surpass the established domain, resulting in a comprehensive collection of centerlines that encapsulate the bifurcation-convergence structure of distributary systems.

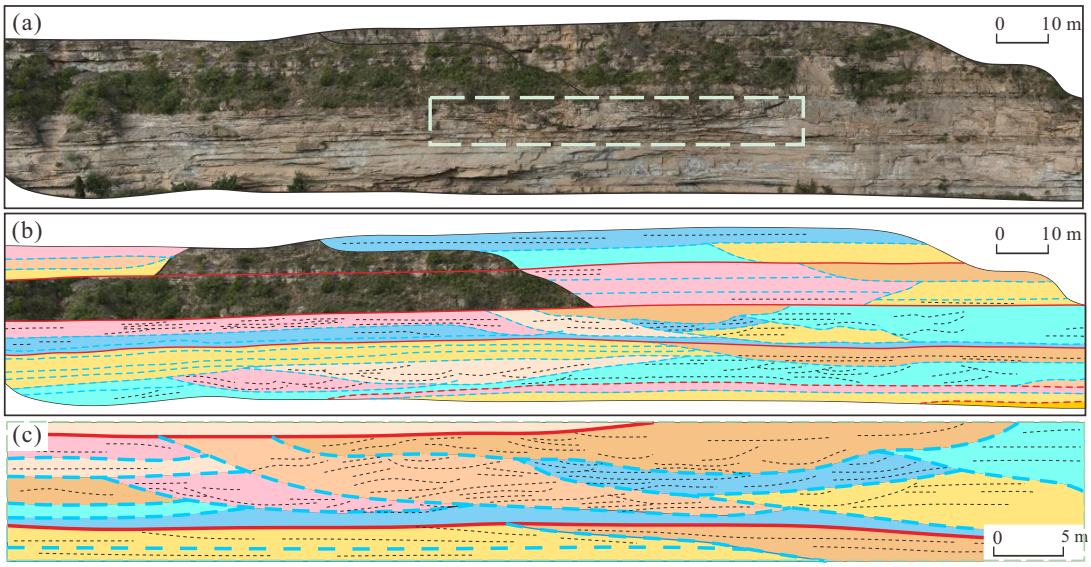

Fig. 6. Interpretation results of subaqueous distributary channels in the Yanchang Formation. (a) Field outcrop photograph, (b) interpreted results and (c) detailed interpretation of the boxed area in (a).

3.1.3 Grid population based on spatial relationships

Subsequent to the creation of the channel vector line collection, the 3D grid is populated in accordance with its spatial relationship to these vectors. A two-dimensional (2D) buffer analysis is conducted for each grid node within the model domain in relation to the channel centerlines (Fig. 5(c)). This analysis ascertains if a grid node is situated within the buffer zone of any channel. Should this occur, the minimal distance from the node to the channel centerline (dmin in Fig. 5(c)) is computed. The distance is thereafter compared to the specified channel width to see whether the node resides within the channel boundary. Nodes inside the channel width are assigned a vertical attribute (e.g., facies type) according to the established channel cross-sectional geometry (Fig. 5(d)). By implementing this iterative procedure on each grid node and assessing their relative positions with all channel vector lines, a comprehensive 3D gridded facies model is generated, thereby establishing the conceptual reservoir model for the shallow-water delta.

3.2 Artificial modeling of sedimentary facies

3.2.1 Construction of 3D training datasets

To achieve a balance between computing efficiency and the modeling precision necessary for the research region, the training dataset grid was configured to dimensions of $96 \times 64 \times 32$ cells, with a resolution of 50 m $\times$ 50 m $\times$ 0.5 m. Facies models were built using the specified grid parameters by implementing the proposed algorithm for conceptual model construction. Simultaneously, supplementary training datasets that included well-point conditions and seismic limitations were developed.

Field outcrops offer significant benefits for geological research, such as direct visibility, dependability, high resolution, and comparatively inexpensive acquisition expenses. They provide essential in-situ information and fundamental geological characteristics for dataset generation. The Triassic Yanchang Formation Chang 6 Member in the Yan'an region of the Ordos Basin is prominently exposed and corresponds to the same stratigraphic interval as the target reservoir, rendering it an exemplary outcrop analogue. Data from 16 channels, oriented perpendicular to the paleo-sediment source direction over 5 profiles, were compiled through systematic observation, measurement, and analysis of these outcrops (Fig. 6) to define channel geometry. Statistical study indicates that channel thickness varies from 2.45 to 9.43 m (mean: 6.13 m), width varies from 25.26 to 382.47 m (mean: 110.70 m), and width-to-thickness ratios range from 9.75 to 58.93 m (mean: 18.26 m) (Fig. 7).

Outcrop data are intrinsically confined and imperfect because to varied exposure, preservation conditions, and the influence of post-depositional events (e.g., tectonic deformation, weathering). As a result, they are unable to accurately depict the three-dimensional geographical distribution of subsurface reservoirs. Contemporary sedimentary analogs, derived from brief observations, markedly contrast with ancient systems that developed over millions of years due to sustained crustal movement and compaction. Consequently, to acquire planar characteristic parameters for model development, this work supplemented outcrop data by extracting channel centerlines from existing sedimentary facies maps. Channels were classified based on their bifurcation hierarchy, and bifurcation angles and spacing underwent statistical analysis across several hierarchical levels within the shallow-water delta system (Table 1).

Conditional reservoir geological modeling utilizing GANs necessitates training the generator on both conceptual models to comprehend geological patterns and on conditional datasets to internalize constraint rules. For the well-point condition dataset, several well locations were randomly chosen through-

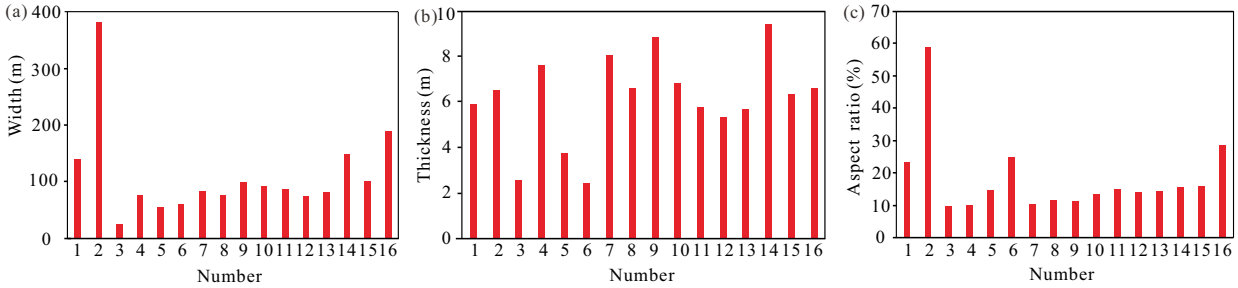

Fig. 7. Quantitative statistics of outcrop channel geometries. Distribution of (a) channel width, (b) channel thickness and (c) channel aspect ratio.

Table 1. Statistical characteristics of channel planar geometry.

Parameters	Bifurcation order				
	1	2	3	4	5
Minimum bifurcation spacing (m)	130	130	240	350	300
Maximum bifurcation spacing (m)	2,500	1,950	2,030	1,450	1,400
Mean bifurcation spacing (m)	925	856	833	789	758
Minimum bifurcation angle (°)	15	15	18	18	21
Maximum bifurcation angle (°)	40	49	43	52	37
Mean bifurcation angle (°)	30.71	27.27	26.61	28.25	31.60

out the conceptual model plane with a stochastic function. The vertical grid columns at these sites were subsequently extracted to develop conditional well models (Fig. 8, third row). An indicator-Gaussian smoothing technique was utilized to construct a reservoir forward model for the seismic probability volume condition dataset. Grid cells in subaqueous distributary channels were designated a value of 1, lateral channel margin cells 0.65, and distributary areas 0. The processed model was further convolved with a specified 3D Gaussian kernel and subjected to random noise perturbation to produce an approximate 3D probability volume, which functions as the conditional dataset (Fig. 8, fourth row). The Gaussian convolution kernel size was randomly chosen between $5 \times 5 \times 13$ and $11 \times 11 \times 25$ grids, taking into account the grid dimensions and standard seismic resolution, to replicate different levels of blurriness in practical seismic probability volumes. The vertical kernel size was proportionately increased to accommodate grid anisotropy. This method cites the approach of Song et al. (2022) in their GANSim-3D research (Section 4.3).

3.2.2 CPGAN framework

The CPGAN framework is constructed upon the GANSim architecture (Song et al., 2021b), as depicted in Fig. 9. The conditioning module comprises two separate components: A global label conditioner and a well-seismic constraint conditioner. The former is executed using a conditional GAN (cGAN) technique, whilst the latter is imposed by a uniquely formulated conditional loss function.

Conditional generative adversarial network for global feature integration. The cGAN architecture incorporates supervised learning principles into the generative process, allowing the generator to create outputs based on specified input labels. Fig. 9 illustrates that both the generator (G) and the discriminator (D) are provided with an additional conditional input y, which denotes a global feature parameter vector. During training, the generator utilizes a random noise vector z along with y to generate a synthetic facies model $G(z|y)$. The discriminator subsequently assesses pairs of data and conditions, differentiating between authentic pairs (x, y) from the training set and synthetic pairs $(G(z|y), y)$. In this adversarial process, the generator progressively enhances its capacity to create facies models that both replicate geological patterns and align with the designated global conditioning parameters.

Gradual integration of well-seismic constraints. In the advancing development of the GAN (CPGAN) architecture, both well and seismic conditioning data are incorporated into the generator beginning at the second resolution layer. A resolution-matching technique is implemented to synchronize the conditioning data with the differing resolutions at various training phases. Well location masks are downsampled via max-pooling to maintain structural integrity, whereas well attribute values and seismic probability volumes are downsampled through average pooling. The downsampled well masks are subsequently multiplied by the associated attribute values to exclude non-well grid cells. The conditioned well data is integrated with the processed seismic volume to generate resolution-specific conditioning inputs. The intermediate feature maps from the generator are concatenated at relevant layers and subjected to additional convolutional procedures.

Conditional loss for the enforcement of constraints. A

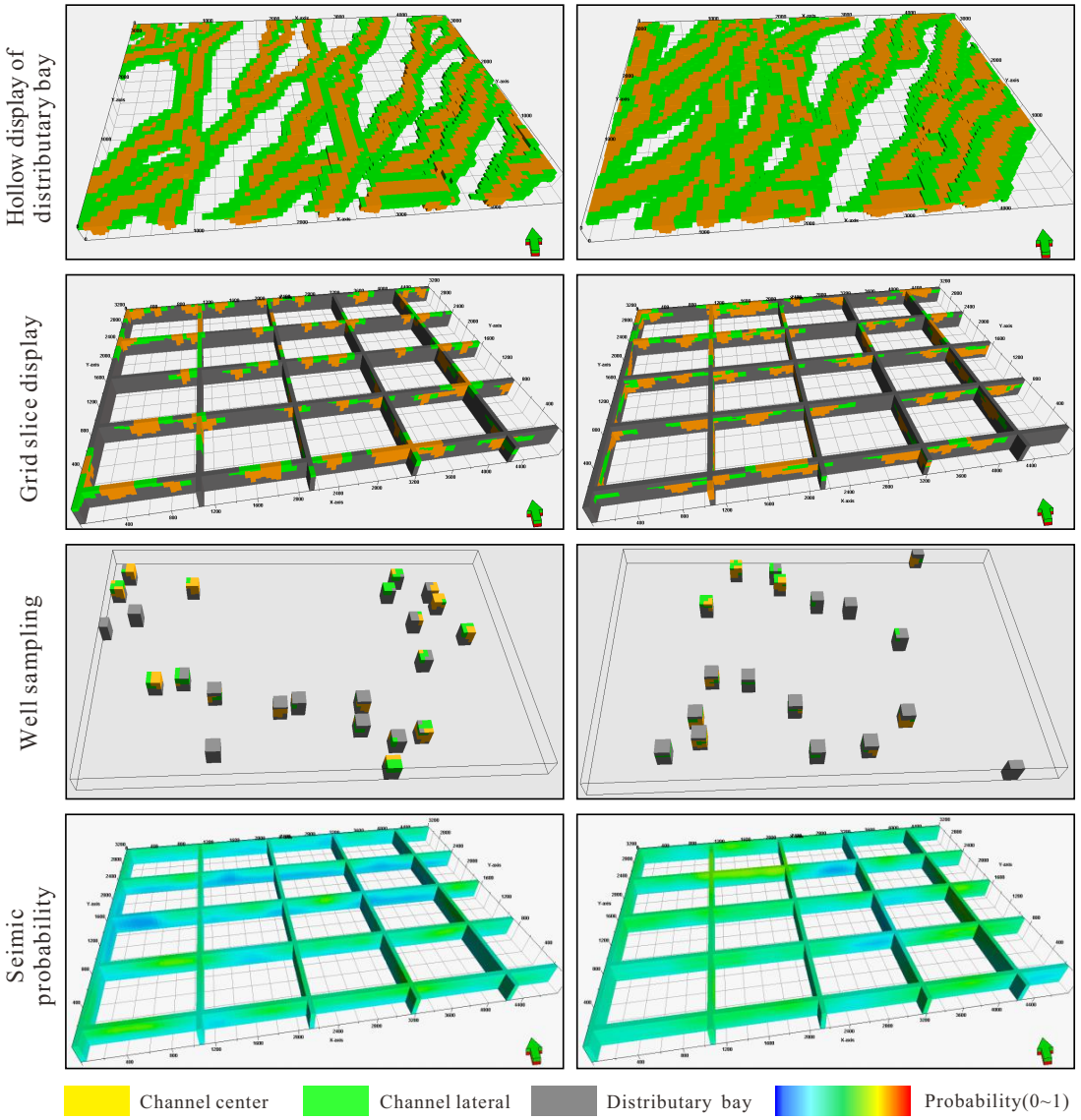

Fig. 8. Shallow-water delta training dataset. Each column represents one set of conditional training data. Rows 1-2 show conceptual microfacies models in different display modes. Row 3 shows well data, and row 4 shows seismic probability.

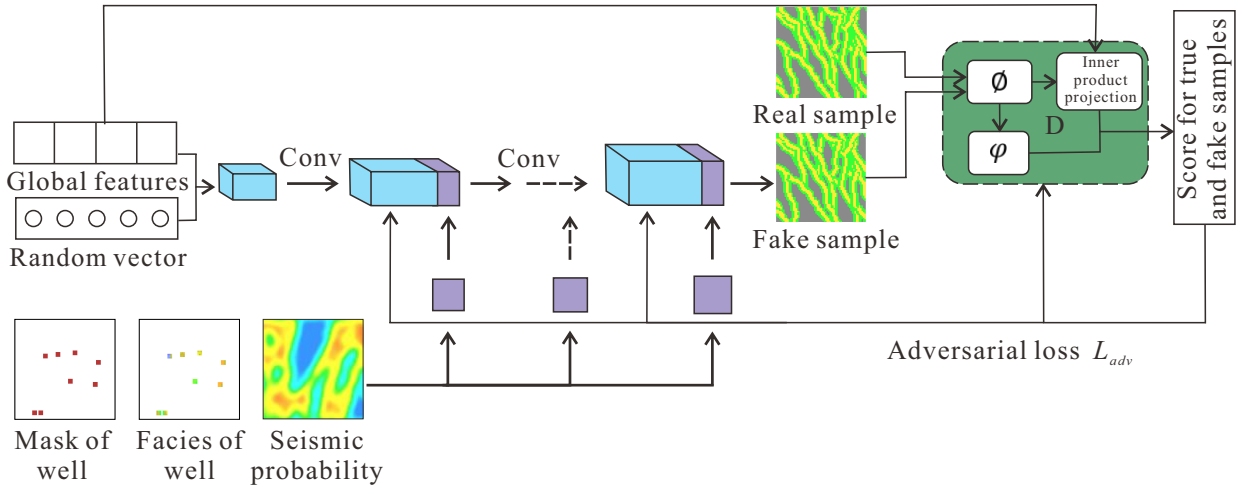

Fig. 9. Architecture of the CPGAN.

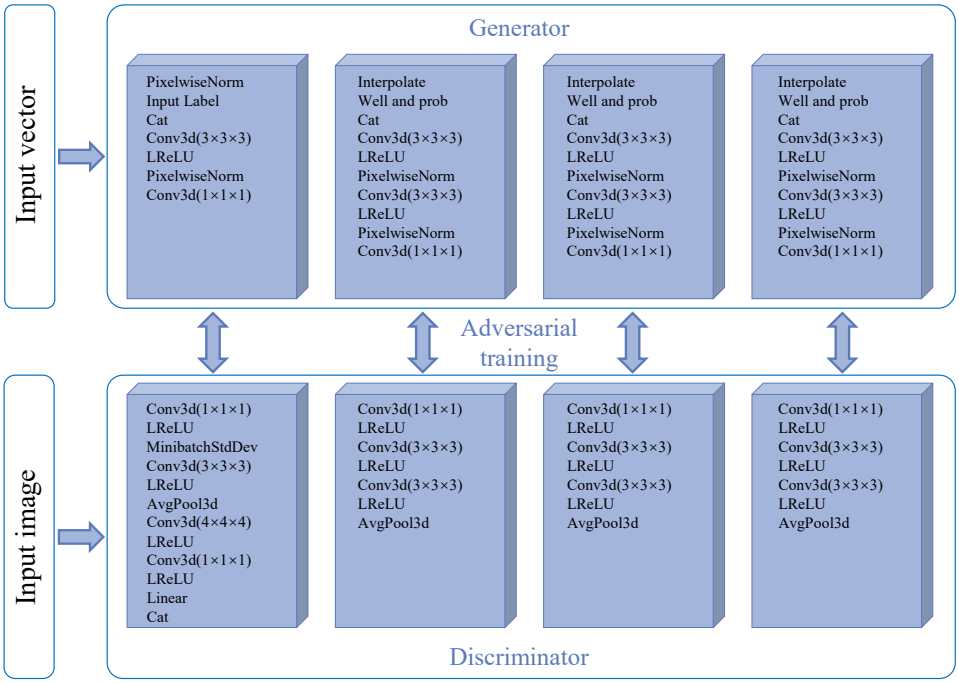

Fig. 10. 3D CPGAN structure (Well and prob represents well and seismic condition data).

conditional loss function is computed during training to impose stringent data limitations. For seismic constraints, a probability volume is derived from the generator's output geological model utilizing the identical forward modeling operator (e.g., indicator-Gaussian smoothing) applied during the training dataset building. Property values for well constraints are immediately taken from the produced model at specified well locations. The conditional loss is calculated as the disparity between the retrieved values and the original conditioning data (the input well/seismic volumes). The loss is backpropagated to refine the generator's parameters, directing it to adhere to the well and seismic limitations while concurrently assimilating the fundamental geological patterns from the conceptual models.

3.2.3 Network architecture, training strategy, and validation

The architectures of the 3D progressive generative adversarial network (CPGAN) generator and discriminator for shallow-water delta modeling are extensively described in Fig. 10. The generator, a fully convolutional neural network, generates an output volume with dimensions $96 \times 64 \times 32$, where the final value in the 'Output shape' column indicates the number of feature channels. In the generator's First Block, "Cat" signifies the channel-wise concatenation of the input random noise vector with a global conditioning label, which is a scalar indicating the ratio of distributary bay facies to regulate the net-to-gross ratio. In the discriminator's Final Block, "Linear" denotes a fully connected layer where the input dimension corresponds to the number of conditioning labels, and the output dimension aligns with the number of features in the final convolutional layer. The ultimate discriminator score is calculated using a weighted aggregation of the convolutional features and the output from the linear layer. Both networks employ 3D convolutional layers utilizing $1 \times 1 \times 1$ kernels and Leaky ReLU activation functions.

The progressive training strategy employs a systematic approach, advancing from low to high resolution. The preliminary network consists solely of the generator's First Block and the discriminator's Final Block. Increased resolutions are attained by progressively incorporating additional General Block modules. During resolution transitions, the output from a lower-resolution layer is upsampled and utilized as input for the subsequent layer. A dedicated $1 \times 1 \times 1$ convolutional layer at the conclusion of each generator block guarantees that the output aligns with the goal resolution for the current training phase; this layer is progressively eliminated when the subsequent, higher-resolution block is integrated. In contrast, a $1 \times 1 \times 1$ convolutional layer assimilates the input at the current resolution into the discriminator. Beginning with the second block, well and seismic conditioning data are merged by channel-wise concatenation (Cat) within the generator. The initial three-channel conditioning data (well mask, well characteristics, seismic probability) is downsampled and integrated into two channels prior to concatenation. The completed network comprises five incrementally expanding layers, with spatial resolution doubling at each stage from an initial $12 \times 8 \times 4$ to a final $96 \times 64 \times 32$.

The CPGAN-based modeling system incorporates geological information of shallow-water delta patterns for parameter optimization and the training process via the generator, while utilizing conditional data through a cGAN mechanism. The training was performed using the PyTorch framework on an NVIDIA RTX 4090D GPU.

The model was trained on a dataset including 5,000 three-dimensional conceptual models. Systematic testing revealed

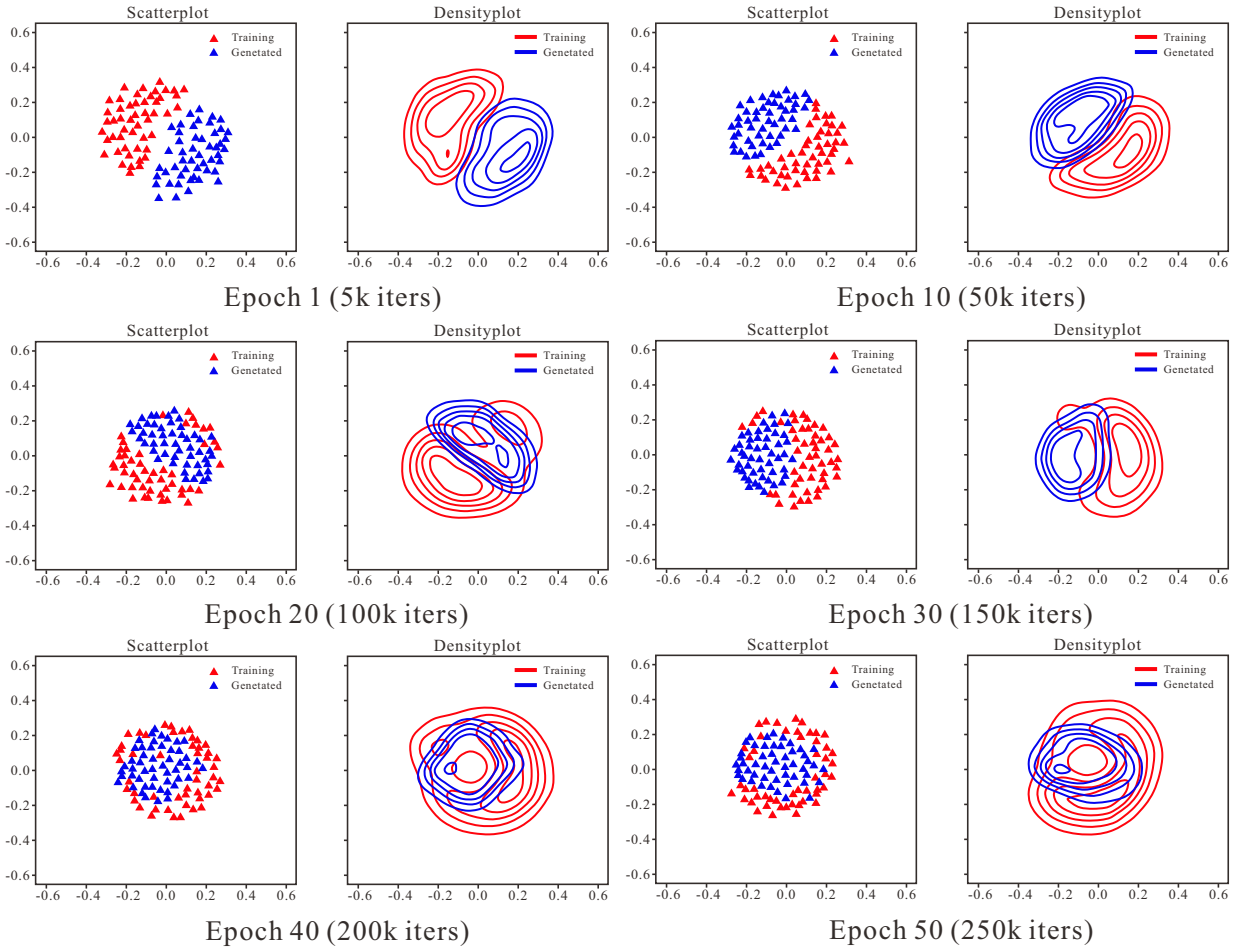

Fig. 11. 2D MDS analysis showing the distribution of generated facies models (blue) and conceptual training models (red) at different training iterations.

Table 2. Training parameters for conditional simulation.

Training parameters	Value
Generator learning rate	0.001
Discriminator learning rate	0.001
Exponential moving average decay factor	0.999
Generator training iterations per discriminator update	1
Discriminator iters per batch	1
Maximum training iters	100
Percentage of iters for new layer fade-in	20%
Original adversarial loss function weight	1
Well point loss function weight	1,000
Seismic probability volume loss function weight	0.000001
Number of global tag parameters	1

that network convergence stabilizes at around 5,000 samples, with bigger training sets providing very minimal quality enhancements while greatly escalating computing expenses. Following comprehensive testing and hyperparameter optimization, the conclusive training parameters for the research region are presented in Table 2. The well point loss weight (1,000) and the seismic probability volume loss weight (0.000001) exhibit substantial differences owing to their unique spatial scales: The well loss denotes specific matching inaccuracies at defined well locations, whereas the seismic loss indicates fitting discrepancies throughout the entire grid. The well's weight loss of 1,000 guarantees about 100% conditioning at well sites, emphasizing these direct geological findings with great dependability. The reduced seismic loss weight (10^{-6}) functions as a soft constraint that directs extensive spatial trends, averting undue diminishment of model diversity while allowing for ambiguities in seismic interpretation. The weight coefficients facilitate scale normalization, equilibrating their contributions to the overall loss function. The training process was evaluated utilizing the Multi-Scale Sliced Wasserstein Distance metric (Song et al., 2021a) and qualitative visual analysis.

The training process's convergence was assessed both quantitatively and qualitatively. A 2D multidimensional scaling (MDS) analysis (Fig. 11) illustrates the distribution of generated facies models relative to the conceptual training models at different training stages. The distributions exhibit

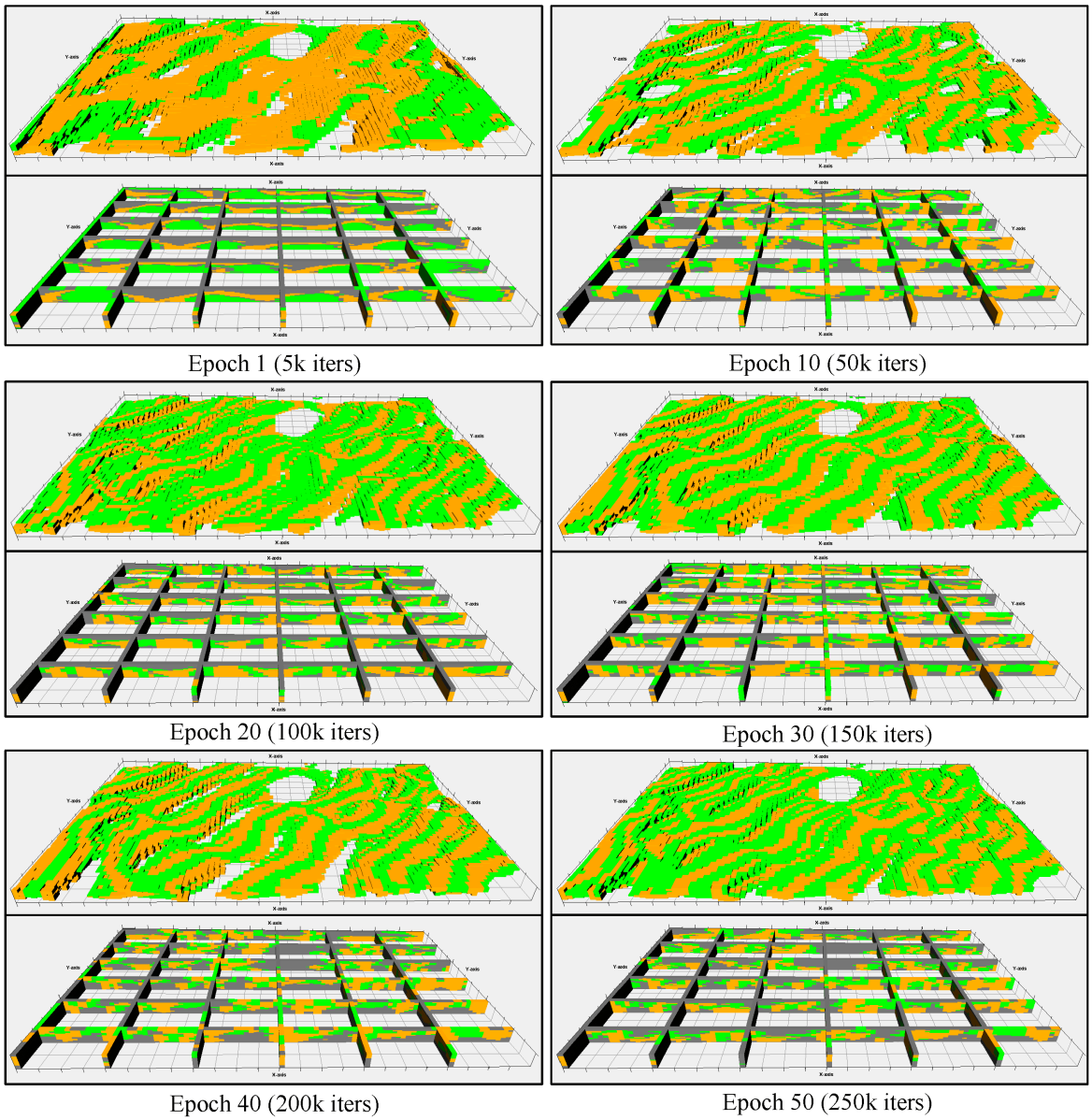

Fig. 12. Realizations of microfacies models generated at different training iterations. In each epoch, the first row shows a hollow display of the distributary bay, and the second row indicates the grid slice profile.

gradual convergence, effectively amalgamating after roughly 40 repetitions. A qualitative visual evaluation of the generated realizations (Fig. 12) validated that the models produced after 50 iterations displayed geological properties that were highly congruent with the conceptual training pictures while adhering to the input limitations. Consequently, training concluded after 50 iterations, and the generator from this phase was preserved for future reservoir facies modeling. The entire 50-iteration training procedure necessitated roughly 35 hours of computing.

4. Results and discussion

4.1 Results analysis of the artificial facies model

The study area covers roughly 50 km^2. Geological modeling was conducted on an area measuring 7,700 m × 6,500 m × 43.5 m, discretized into a grid of 155 × 130 × 87 cells with a resolution of 50 m × 50 m × 0.5 m. Given that this domain surpasses the dimensions of the training dataset (96 × 64 × 32 grids), the trained CPGAN generator was adjusted to accommodate the wider study region. The scaling factors of 1.61, 2.03, and 2.72 were applied to the dimensions of the input latent vector in the x, y, and z directions, respectively. The network output was produced at progressively increased resolutions (40 × 34 × 22, 80 × 68 × 44, and ultimately 160 × 136 × 88), followed by the trimming of grids that extended beyond the intended model border (Fig. 13).

The trained CPGAN generator was utilized for conditional simulation. The analysis of upscaled well log statistics indicated that the distributary bay facies constitute roughly 38% of the target period. The global parameter, in conjunction with the enhanced well conditioning data and the seismic

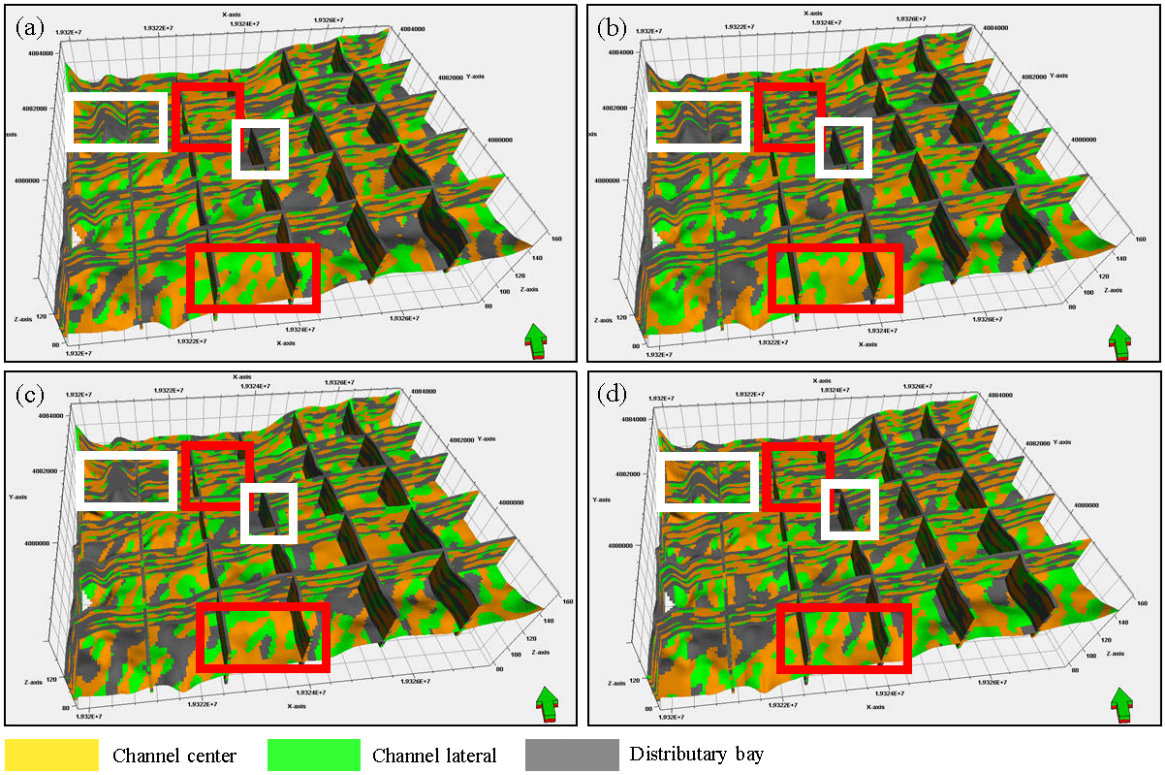

Fig. 13. Four stochastic realizations of the shallow-water delta sedimentary microfacies model generated by the CPGAN, showing the distribution of subaqueous distributary channels (red/yellow), lateral margins (blue), and distributary bays (transparent). White and red boxes indicate areas for comparison with the seismic probability volume. (a) Stochastic realization 1, (b) stochastic realization 2, (c) stochastic realization 3 and (d) stochastic realization 4.

probability volume, was input into the generator to create several equiprobable realizations of the sedimentary facies model for the Wangyao Block.

Four stochastic realizations of the shallow-water delta sedimentary microfacies model were presented with partial transparency and slicing to expose internal architecture (Fig. 13). The simulated models exhibit strong alignment with the geological patterns acquired during training. In plan view, subaqueous distributary channels demonstrate frequent bifurcation and convergence, resulting in laterally amalgamated channel complexes. Channel bodies are bordered by slender, laterally extended edges, precisely mirroring the original design. The models distinctly illustrate the typical vertical stacking pattern in cross-section, featuring heavier channel sands interspersed with distributary mudstones and slender peripheral deposits.

A comparison of the simulated facies models (Fig. 13) and the constraining seismic probability volume (Fig. 14(b)) validates the successful integration of seismic data. Regions characterized by distributary bay facies in the models (shown by white boxes in Fig. 13) consistently align with areas of low likelihood in the seismic volume. In contrast, areas dominated by subaqueous distributary channels (shown by red boxes in Fig. 13) correspond with high-probability locations in Fig. 14(b). This illustrates the effectiveness of the conditional loss function in guiding the generator to adhere to the soft seismic limitations.

Although all four realizations are based on the same well and seismic data, they are not identical, as they were produced from distinct random latent vectors. The observed heterogeneity in the spatial arrangement of channels and margins reflects a plausible range of geological uncertainty, demonstrating the model's capacity to produce several, equally probable reservoir descriptions that align with the available data.

The well interpretation data, coarsened to the modeling grid (Fig. 14(a)), served as hard constraints during conditional simulation. Traditional pixel-based techniques achieve complete (100%) well-point conditioning by directly allocating values at well sites, while CPGAN concurrently acquire geological patterns and conditioning restrictions through a conditional loss function. This mechanism has difficulties in attaining comprehensive data fidelity while maintaining geological pattern integrity in densely networked well conditions, requiring a compromise between pattern preservation and conditioning precision. Fig. 15(a) displays the unrefined microfacies model output generated by the CPGAN. Despite an overall conditioning rate of approximately 93% (Fig. 15(b)), unrealistic local disturbances (indicated by the red arrow in Fig. 15(a)) and substantial noise artifacts arise near well locations, illustrating that the generator insufficiently reconciles conditioning constraints with geological continuity. Thus, CPGAN-generated microfacies models generally necessitate model selection and post-processing techniques to achieve geologically plausible final realizations.

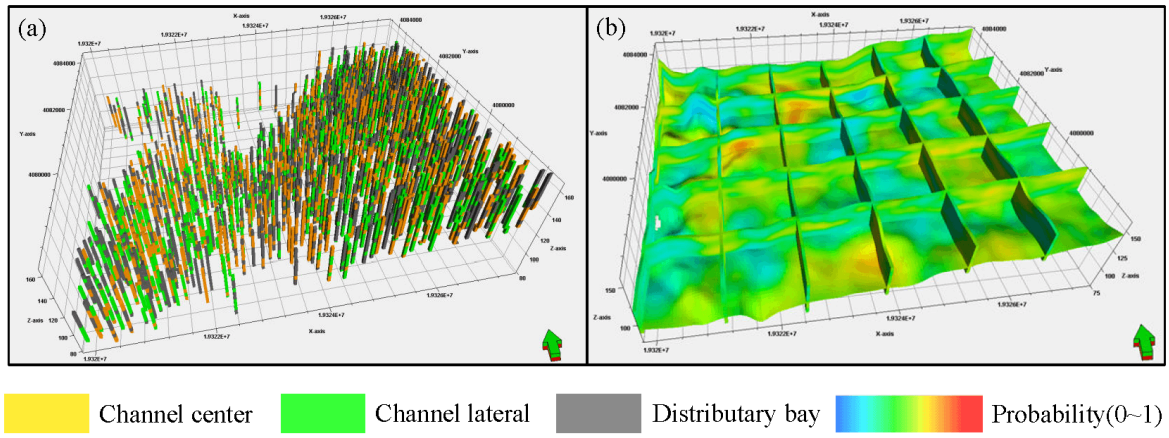

Fig. 14. (a) Coarsening well interpretation data to grid and (b) seismic probability volume for subaqueous distributary channel facies in the study area. Both figures are used as soft constraints during conditional simulation.

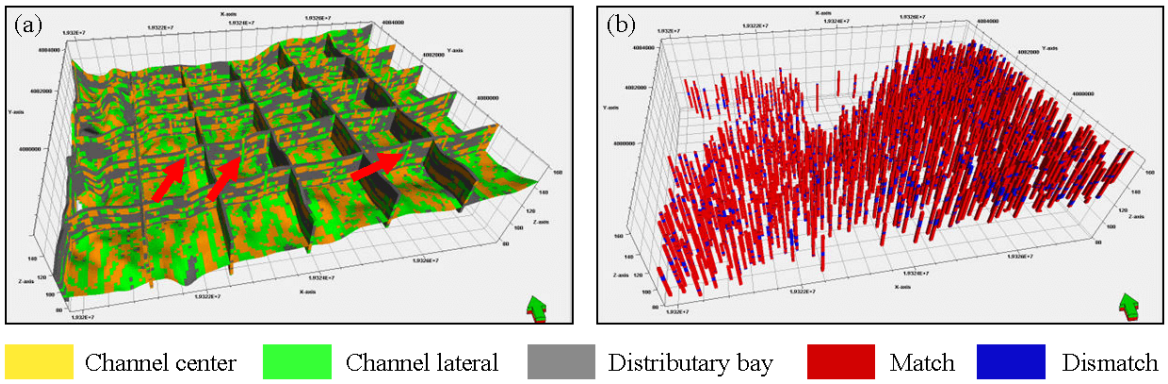

Fig. 15. (a) Unprocessed microfacies model output from the CPGAN and (b) grid-by-grid matching between well interpretation and microfacies model.

Table 3. Comparison of average simulation times (s) for different methods.

Method	Number of grids (million)		
	1	10	100
CPGAN	0.6	1.6	20
SIMPAT	90	180	720
SNESIM	180	420	1,200
SISIM	45	120	300

4.2 Methods comparison

To statistically assess the suggested technique, thirty training image groups were randomly chosen from the dataset. Each group developed 100 geological realizations utilizing the MPS and sequential indicator simulation modules in Petrel 2022 software. Thirty realizations were randomly chosen from each set of 100 models, and the Multi-Scale Sliced Wasserstein Distance metric was utilized to evaluate the quality of models generated by various approaches. Fig. 16 illustrates that the CPGAN-generated realizations demonstrate a distribution pattern that more accurately resembles the training picture groups in comparison to traditional approaches. The computational efficiency of each method was assessed by determining the average generation time per realization across various grid resolutions (Table 3). The CPGAN method exhibits computational accelerations of one to two orders of magnitude (tenfold to hundredfold) compared to conventional geostatistical techniques. The specifications of the test computer are as follows: 13th Gen Intel Core i7-13700KF (3.40 GHz); RAM: 64.0 GB (4,200 MHz). During the CPGAN inference phase, the GPU variant of LibTorch, the deployment tool for PyTorch, was utilized without the involvement of a graphics card.

4.3 Reserves calculation and model validation

Reserves represent a cohesive representation of essential reservoir properties, such as effective porosity, water saturation, and net-to-gross ratio. Consequently, the precision of reserve estimation functions as a vital and thorough validation criterion for the foundational geological and petrophysical models. Utilizing the developed facies model, facies-controlled sequential indicator simulation was employed to create appropriate porosity and water saturation models for the research region.

The effective porosity in the model varies from 3.4% to 24.4%, with an average of 13.30%. The water saturation va-

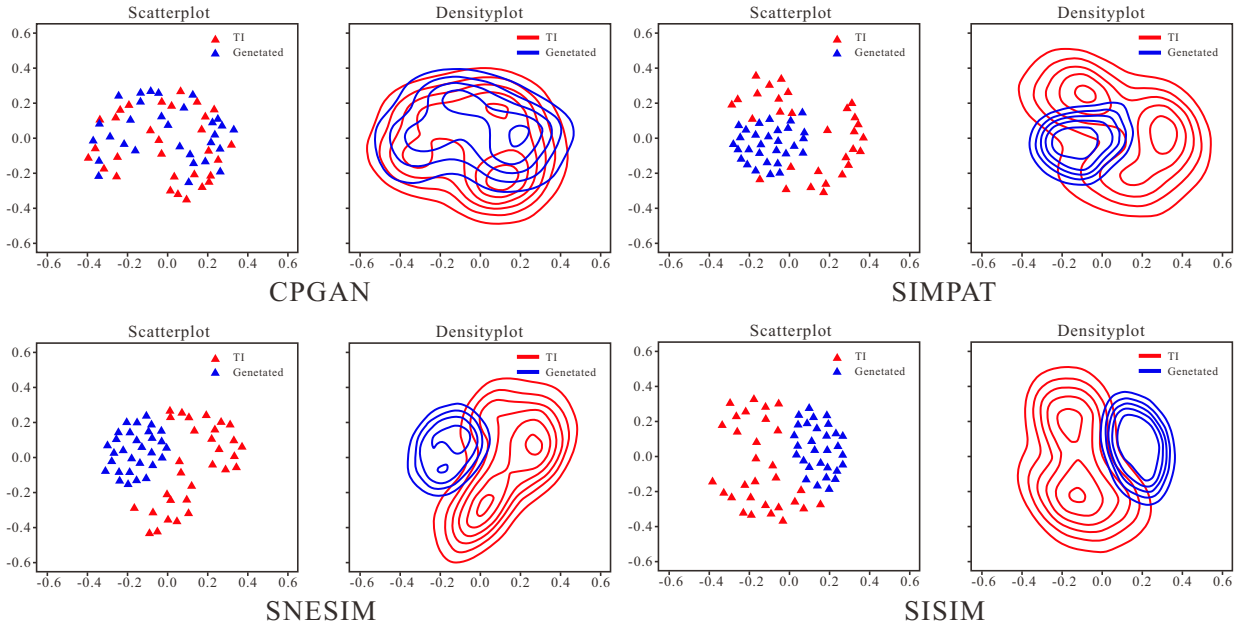

Fig. 16. MDS analysis using different methods.

Table 4. Reserve estimation results from geological model realizations of Fig. 13.

No.	Reserves (10^4 t)	Error (10^4 t)	Relative error (%)
1	3,534.16	148.99	4.40
2	3,221.16	-164.01	-4.84
3	3,623.89	238.72	7.05
4	3,215.15	-170.02	-5.02

lues, limited by core-derived statistics, vary from 33.33% to 52.60%. The initial oil in place was subsequently determined from the geological models.

To validate the models, the computed reserves from four realizations were juxtaposed with the measured average reserves from well groups ($3{,}385.17 \times 10^4$ t). The findings, presented in Table 4, indicate that the estimation errors for all realizations are within $\pm 10\%$. This tight agreement illustrates the exceptional precision and dependability of the produced geological models in depicting the underlying reservoir volume.

5. Conclusions

This research illustrates the efficacy of a cohesive approach that merges process-informed, vector object-based modeling with a Conditional Progressive Generative Adversarial Network (CPGAN) for the precise characterisation of shallow-water delta reservoirs. The principal conclusions are:

1) The suggested vector object-oriented approach effectively encapsulates the intricate bifurcation and bifurcation and convergence patterns of subaqueous distributary channels, facilitating the rapid creation of geologically authentic 3D training datasets.
2) The enhanced CPGAN framework efficiently amalgamates multi-source data, encompassing global geological parameters, well logs, and seismic probability volumes, into a unified process. It produces several equiprobable facies realizations that faithfully adhere to hard data limitations while maintaining distinctive sedimentary architecture.
3) The application of the approach to a field example in the Ordos Basin corroborates its trustworthiness, as model-derived reserve estimates align closely with historical data, thus affirming its practical utility and precision.
4) The workflow creates a strong and flexible methodological foundation for intelligent reservoir modeling, showing considerable potential for improving modeling accuracy and efficiency in data-limited situations.

Notwithstanding its benefits, the technique has specific limits. The performance is contingent upon system-specific training data and parameterization, potentially influencing instant transferability. Moreover, a significant trade-off occurs between optimal well-conditioning and the maintenance of extensive geological continuity, underscoring a crucial domain for future algorithmic enhancement in deep learning-based geomodeling.

Acknowledgements

This research was supported by the National Science and Technology Major Project for New Oil and Gas Exploration and Development (No. 2025ZD1401502), and the China National Petroleum Corporation (CNPC) Forward-looking and Fundamental Technology Research Project (No. 2023DJ84).

Conflicts of interest

The authors declare no competing interest.

References

Bao, P., Hui, G., Hu, Y., et al. Comprehensive characterization of hydraulic fracture propagations and prevention of pre-existing fault failure in Duvernay shale reservoirs. Engineering Failure Analysis, 2025, 173: 109461.

Cai, J., Xu, K., Zhu, Y., et al. Prediction and analysis of net ecosystem carbon exchange based on gradient boosting regression and random forest. Applied Energy, 2020, 262: 114566.

Chen, G., Jia, Y., Yin, Y., et al. Remote sensing image dehazing using a wavelet-based generative adversarial networks. Scientific Reports, 2025, 15: 3634.

Chen, L., Lu, Y., Wu, J., et al. Sedimentary facies and depositional model of shallow water delta dominated by fluvial for the Chang 8 oil-bearing group of Yanchang Formation in southwestern Ordos Basin, China. Journal of Central South University, 2015, 22(12): 4749-4763.

Chen, Q., Cui, Z., Liu, G., et al. Deep convolutional generative adversarial networks for modeling complex hydrological structures in Monte-Carlo simulation. Journal of Hydrology, 2022, 610: 127970.

Deutsch, C. V., Tran, T. T. FLUVSIM: A program for object-based stochastic modeling of fluvial depositional systems. Computers & Geosciences, 2002, 28(4): 525-535.

Deutsch, C. V., Wang, L. Hierarchical object-based stochastic modeling of fluvial reservoirs. Mathematical Geology, 1996, 28(7): 857-880.

Dong, W., Chen, X., Yang, Q. Data-driven scenario generation of renewable energy production based on controllable generative adversarial networks with interpretability. Applied Energy, 2022, 308: 118387.

Du, S., Bai, L. Future potential research hotspots on the precise integration of geology and engineering in low-permeability oil reservoirs. Advances in Geo-Energy Research, 2024, 14(1): 4-7.

Hou, Q., Wang, F., Meng, Q., et al. Depositional characteristics of shallow water delta in large depression lake basin and control of reservoir distribution. Paper 202011504 Presented at the 82nd EAGE Annual Conference & Exhibition, Amsterdam, The Netherlands, 18-21 October, 2021.

Hu, X., Song, S., Hou, J., et al. Stochastic modeling of thin mud drapes inside point bar reservoirs with ALLUVSIM-GANSim. Water Resources Research, 2024, 60(6): e2023WR035989.

Huang, X., Liu, K., Zou, C., et al. Forward stratigraphic modelling of the shallow-water delta system in the Poyang Lake, southern China. Journal of Geochemical Exploration, 2014, 144: 74-83.

Hui, G., Chen, S., Gu, F. Strike-slip fault reactivation triggered by hydraulic-natural fracture propagation during fracturing stimulations near Clark Lake, Alberta. Energy & Fuels, 2024, 38(19): 18547-18555.

Hui, G., Chen, S., He, Y., et al. Machine learning-based production forecast for shale gas in unconventional reservoirs via integration of geological and operational factors. Journal of Natural Gas Science and Engineering, 2021, 94: 104045.

Hui, G., Chen, Z., Schultz, R., et al. Intricate unconventional fracture networks provide fluid diffusion pathways to reactivate pre-existing faults in unconventional reservoirs. Energy, 2023, 282: 128803.

Hui, G., Ren, Y., Bi, J., et al. Artificial intelligence applications and challenges in oil and gas exploration and development. Advances in Geo-Energy Research, 2025, 17(3): 179-183.

Jia, J., Li, D., Wang, L., et al. Novel transformer-based deep neural network for the prediction of post-refracturing production from oil wells. Advances in Geo-Energy Research, 2024, 13(2): 119-131.

Kavousinejad, S., Dalaie, K., Behnaz, M., et al. Developing an artificial intelligence-based progressive growing GAN for high-quality facial profile generation and evaluation through turing test and aesthetic analysis. Scientific Reports, 2025, 15: 26611.

Laloy, E., Hérault, R., Lee, J., et al. Inversion using a new low-dimensional representation of complex binary geological media based on a deep neural network. Advances in Water Resources, 2017, 110: 387-405.

Liu, H., Qiu, Z., Xu, L., et al. Distribution of shallow water delta sand bodies and the genesis of thick layer sand bodies of the Triassic Yanchang Formation, Longdong Area, Ordos Basin. Petroleum Exploration and Development, 2021a, 48(1): 123-135.

Liu, Q., Xu, J., Jiang, R., et al. Density estimation using deep generative neural networks. Proceedings of the National Academy of Sciences of the United States of America, 2021b, 118(15): e2101344118.

Liu, J., Xian, B., Tan, X., et al. Sub-lacustrine debrite system: Facies architecture and sediment distribution pattern. Petroleum Science, 2025, 22(1): 110-129.

Li, Y., Wu, S., Hou, J., et al. Progress and prospects of reservoir development geology. Petroleum Exploration and Development, 2017, 44(4): 603-614.

Lu, C., Li, S., Wang, X., et al. Combining image editing and SinGAN for conditional sedimentary facies modeling. IEEE Geoscience and Remote Sensing Letters, 2024, 21: 3004704.

Mao, Y., He, Q., Zhao, X. Designing complex architectured materials with generative adversarial networks. Science Advances, 2020, 6(17): eaaz4169.

Mariethoz, G., Caers, J. Multiple-Point Geostatistics: Stochastic Modeling With Training Images. Chichester, UK, Wiley, 2014.

Murgas, B., Stickel, J., Brewer, L., et al. Modeling complex polycrystalline alloys using a Generative Adversarial Network enabled computational platform. Nature Communications, 2024, 15(1): 9441.

Pyrcz, M. J., Boisvert, J. B., Deutsch, C. V. ALLUVSIM: A program for event-based stochastic modeling of fluvial depositional systems. Computers & Geosciences, 2009, 35(8): 1671-1685.

Qi, Y., Wang, Y., Qin, G., et al. Sedimentary evolutionary pro-

cesses, architecture, and sedimentary model of a lobate shallow-water delta: Insights from flume simulation experiments. Frontiers in Earth Science, 2024, 12: 1393211.

Ren, Y., Zeng, C., Li, X., Liu, X., Hu, Y., et al. Intelligent evaluation of sandstone rock structure based on a visual large model. Petroleum Exploration and Development, 2025, 52: 548-558.

Song, S., Mukerji, T., Hou, J. Geological facies modeling based on progressive growing of generative adversarial networks (GANs). Computational Geosciences, 2021a, 25(3): 1251-1273.

Song, S., Mukerji, T., Hou, J. GANSim: Conditional facies simulation using an improved progressive growing of generative adversarial networks (GANs). Mathematical Geosciences, 2021b, 53(7): 1413-1444.

Song, S., Mukerji, T., Hou, J., et al. GANSim-3D for conditional geomodeling: Theory and field application. Water Resources Research, 2022, 58(7): e2021WR031865.

Sun, C., Demyanov, V., Arnold, D. GAN River-I: A process-based low NTG meandering reservoir model dataset for machine learning studies. Data in Brief, 2023, 46: 108785.

Tahmasebi, P. Multiple point statistics: A review, in Handbook of Mathematical Geosciences, edited by B. S. Daya Sagar, Q. Cheng, and F. Agterberg, Springer International Publishing, Cham, pp. 613-643, 2018.

Tang, Z., Qiu, S., Cai, Z., et al. Multi-gate mixture-of-different-experts model for the prediction of multiple properties in multi-phase rocks. Advances in Geo-Energy Research, 2026, 19(2): 182-196.

Wang, L., Yin, Y., Wang, H., et al. A method of reconstructing 3D model from 2D geological cross-section based on self-adaptive spatial sampling: A case study of Cretaceous McMurray reservoirs in a block of Canada. Petroleum Exploration and Development, 2021, 48(2): 407-420.

Wang, X., Jiang, H., Mu, M., et al. A trackable multi-domain collaborative generative adversarial network for rotating machinery fault diagnosis. Mechanical Systems and Signal Processing, 2025, 224: 111950.

Yang, N., Li, G., Li, T., et al. An improved deep dilated convolutional neural network for seismic facies interpretation. Petroleum Science, 2024a, 21(3): 1569-1583.

Yang, T., Li, X., Yang, Y., et al. Evolution from shallow-water deltas to fluvial fans in lacustrine basins: A case study from the Middle Jurassic Shaximiao Formation in the central Sichuan Basin, China. Sedimentology, 2024b, 71(3): 1023-1055.

Zhang, C., Liu, G., Chen, Q., et al. Post-constrained conditional sedimentary facies simulation from a single training image using a concurrent multi-stage generative adversarial network. Water Resources Research, 2025, 61(11): e2025WR040582.

Zhang, T., Yang, Z., Sun, C. Stochastic simulation of fan deltas using parallel multi-stage generative adversarial networks. Journal of Petroleum Science and Engineering, 2022, 208: 109442.

Zhang, T., Tilke, P., Dupont, E., et al. Generating geologically realistic 3D reservoir facies models using deep learning of sedimentary architecture with generative adversarial networks. Petroleum Science, 2019, 16(3): 541-549.

Zhao, J., Wu, J., Wang, H., et al. Single phase flow simulation in porous media by physical-informed Unet network based on lattice Boltzmann method. Journal of Hydrology, 2024, 639: 131501

Zhao, L., Hu, C., Quaye, J. A., et al. Comparative analysis of 3D reservoir geologic modeling: A comprehensive review and perspectives. Geoenergy Science and Engineering, 2025, 244: 213440.

Zheng, X., Shi, J., Cao, G., et al. Progress and prospects of oil and gas production engineering technology in China. Petroleum Exploration and Development, 2022, 49(3): 644-659.

Zhu, X., Zeng, H., Li, S., et al. Sedimentary characteristics and seismic geomorphologic responses of a shallow-water delta in the Qingshankou Formation from the Songliao Basin, China. Marine and Petroleum Geology, 2017, 79: 131-148.